physica status solidi a
www.pss-a.com

Surface Photovoltage Spectroscopy over Wide Time Domains for Semiconductors with Ultrawide Bandgap: Example of Gallium Oxide

Thomas Dittrich, Steffen Fengler, and Norbert Nickel*

A nonconventional approach is proposed for the measurement of surface photovoltage (SPV) signals over very wide ranges in photon energy and time. Regimes for AC, DC, and combined AC–DC measurements are defined and applied for the characterization of a β-Ga_2O_3 crystal by transient and modulated SPV spectroscopy, spectroscopy in the mode of a Kelvin probe and single-pulse SPV transients from 10 ns to 1000 s with the same electrode. Numerous electronic transitions are distinguished in β-Ga_2O_3 depending on the measurement regime, the time response and the history of measurement. An accumulation of negative charge at the surface of β-Ga_2O_3 is observed at long times independent whether the SPV signals are positive or negative before. The nonconventional approach of measuring SPV signals opens new opportunities for investigating electronic properties of semiconductors with ultrawide bandgaps and any other photoactive materials.

1. Introduction

Semiconductors with ultrawide bandgap (E_g), such as Ga_2O_3, can be applied, for example, in power electronics and optoelectronic devices due to their high breakdown voltage and transparency, respectively.[1–3] Aside this, semiconductors with ultrawide bandgap are also of increasing interest for solar energy conversion. For example, Ga_2O_3 layers can serve as passivation, transparent ohmic contact or charge-selective contact layers as shown in solar cells based on Cu(In,Ga)Se_2,[4] c-Si,[5] or Cu_2O[6] absorbers, respectively. Furthermore, Ga_2O_3 is of great interest for photocatalytic water splitting. As very few examples, the role of copper and chromia-based cocatalysts on Ga_2O_3,[7] of mixed-phase junctions based on β-Ga_2O_3/α-Ga_2O_3,[8,9] of zinc and lead dopants in Ga_2O_3[10] or of nickel oxide cocatalysts on α-Ga_2O_3[11] for photocatalytic activity and photocatalytic water splitting were investigated empirically and by first-principle studies, respectively.

Electronic states in the bandgap are crucial for the operation of electronic, optoelectronic, solar cell, and photocatalytic devices. Therefore, the characterization of electronic states and the study of their interactions is decisive for the engineering of electronic states and the further development of devices. Energy levels of deep defect states in Ga_2O_3 were obtained using deep-level transient spectroscopy (DLTS)[12,13] and Hall effect measurements at high temperatures.[14] Several transition energies were measured by cathodoluminescence spectroscopy.[15] However, reliable data about defect states and electronic transitions in Ga_2O_3 are sparse and the characterization of electronic transitions and their impact on electronic properties of semiconductors with ultrawide bandgap over the entire E_g is often challenging.

Surface photovoltage (SPV) techniques provide universal tools for the highly sensitive analysis and investigation of electronic states in semiconductors.[16,17] Recently, for example, transitions and charge transfer processes were studied in c-Si/TiO_2 and $CuBi_2O_4$ heterojunctions by transient[18] and modulated[19] SPV spectroscopy, respectively, and the bulk photovoltaic effect has been shown for excitation from defect states in carbon-doped GaN.[20] Incidentally, one SPV spectrum has been shown for Ga_2O_3 in the work of Gao et al.,[15] but in our opinion, the signal-to-noise ratio was insufficient to extract energy levels in a reliable manner.

Fast and robust SPV measurements are carried out in the fixed capacitor arrangement[21] for achieving short resolution times (below 1 ns,[22] transient measurements) or high sensitivity (range of 100 nV,[23] modulated measurements). In the fixed capacitor arrangement, an electrode based on a transparent conducting oxide (TCO) and an insulating foil between the sample and the electrode are used for forming the measurement capacitor for capacitive out-coupling of SPV signals. However, optical absorption in the TCO electrode and in the insulating foil avoid the application of conventional fixed capacitor arrangements for SPV measurements on semiconductors with ultrawide bandgaps.

In this work, a fine gold mesh electrode was kept at a certain distance to the sample surface for performing transient and

T. Dittrich, N. Nickel
Helmholtz-Zentrum Berlin für Materialien und Energie GmbH
Institut für Si-Photovoltaik
Kekulé Str. 5, 12489 Berlin, Germany
E-mail: dittrich@helmholtz-berlin.de

S. Fengler
Helmholtz-Zentrum Hereon GmbH
Max-Planck-Str. 1, 21502 Geesthacht, Germany

The ORCID identification number(s) for the author(s) of this article can be found under https://doi.org/10.1002/pssa.202100167.

© 2021 The Authors. physica status solidi (a) applications and materials science published by Wiley-VCH GmbH. This is an open access article under the terms of the Creative Commons Attribution License, which permits use, distribution and reproduction in any medium, provided the original work is properly cited.

DOI: 10.1002/pssa.202100167

© 2021 The Authors. physica status solidi (a) applications and materials science published by Wiley-VCH GmbH

modulated SPV measurements (AC regime). As the capacitance of such a measurement configuration is relatively small, the conventional measurement principle of direct capacitive outcoupling of potentials with a high impedance buffer would induce too much noise, the conventional fixed capacitor arrangement was replaced by the principle of charge measurement with a highly sensitive charge amplifier. Incidentally, for ac SPV measurements with a charge amplifier, the potential response shall be calibrated with an external source.

The SPV measurement configuration with a charge amplifier and a gold mesh electrode allows also for SPV measurements in the Kelvin-probe regime (the contact potential difference [CPD] is measured,[16] DC regime) and for combined transient SPV and Kelvin probe measurements over extremely wide time ranges after single-pulse excitation (combined AC–DC regime).[24]

In this work, the high potential of the measurement principle of SPV signals with highly sensitive charge amplifiers was demonstrated by measurements of transient and modulated SPV spectroscopy, SPV spectroscopy with a Kelvin-probe and transient SPV over extremely wide time ranges with the same electrode for a β-Ga_2O_3 single crystal. Based on sign and relaxation of spectral-dependent SPV signals, a variety of known and unknown defect-related transitions were distinguished for trap states in the bulk and at/near the surface of β-Ga_2O_3.

2. Experimental Section

2.1. Electrode Configuration

A conventional Kelvin probe with a fine gold mesh (diameter 3 mm) and a piezoelectric oscillator (delta Phi Besocke) was modified by adding a grounded shield up to the level of the electrode and a highly sensitive charge amplifier just on top of the electrode. Analog electronics were developed and realized by Franke for conducting 1) transient SPV measurements (AC regime), 2) measurements of CPD (DC regime), and 3) combined measurements over extremely wide time ranges (AC–DC regime). The average distance between the electrode and the sample surface was adjusted with a micrometer screw. **Figure 1** shows the electronic scheme of the measurement configuration.

2.2. AC Regime

Transient and modulated SPV spectroscopy measurements were carried out in the AC regime with an oscilloscope card (Gage, CSE 1622-4GS) and a tunable Nd:YAG laser for excitation (duration time of laser pulses 3–5 ns, range of wavelengths 216–2600 nm, EKSPLA, NT230–50, equipped with a spectral cleaning unit) and with a lock-in amplifier (EG&G 5210) and a modulated light source (Xe lamp with a SPM2 quartz prism monochromator and an optical chopper), respectively. Quartz prisms and quartz lenses were used for directing and forming the light beams.

In the AC regime, the position of the electrode was fixed, i.e., vibration of the mechanical oscillator was switched off. For calibrating the AC response, a periodic square wave signal with a frequency of $f_{cal} = 22$ Hz and 1 V_{pp} was applied. A corresponding amplification factor (K_{ac}) was defined by measuring the output calibration signal with an oscilloscope. K_{ac} depended on the distance between the electrode and the sample surface (for the measurements an average distance of about 0.2 mm was chosen). During the measurement, the calibration signal was disconnected.

The resolution time was 7 ns in the AC regime. The broadband noise was about 3 mV_{pp} for the AC regime. For the

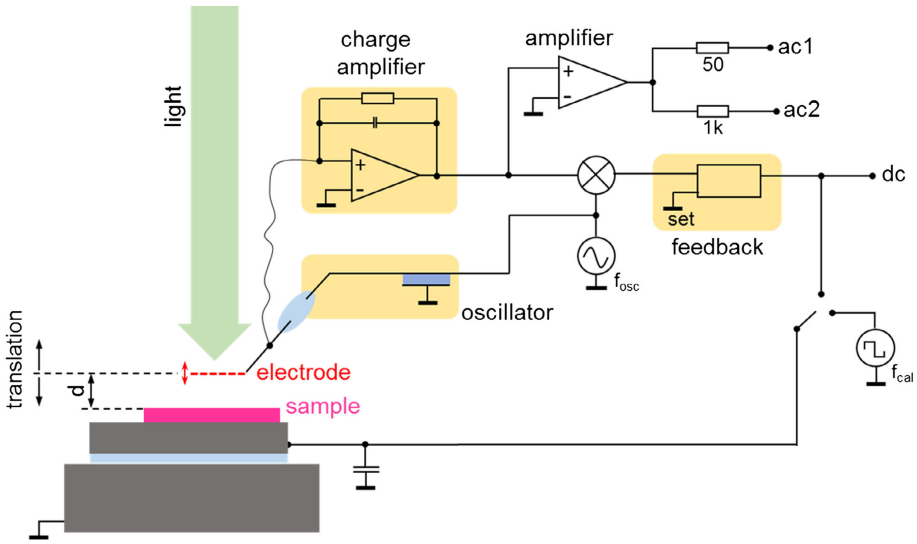

Figure 1. Electronic scheme of the electrode and measurement configurations consisting of the sample and the electrode which form the measurement capacitor, the mechanical oscillator driven by the generator at the frequency f_{osc}, the charge amplifier converting the electrode current to a potential, the amplifier with the decoupled ac1 (short times) and ac2 (intermediate times) outputs, the rectifier and the feedback unit for nulling the electrostatic potential at the measurement capacitor with the DC output. The sample holder can be disconnected from the feedback and connected with a second generator giving a defined square wave at the frequency f_{cal} for the calibration of the AC outputs. The average distance between the electrode and the sample surface is adjusted mechanically with a linear translation element (d).

© 2021 The Authors. physica status solidi (a) applications and materials science published by Wiley-VCH GmbH

transient SPV spectroscopy measurements, the repetition rate of the laser pulses was 1 Hz and ten transients were averaged for one transient which led to a reduction of noise to about 1 mV_{pp} at the shortest times. The noise decreased further with increasing time due to the increasing number of samples for averaging for the logarithmic read-out.

2.3. DC Regime

CPD measurements were carried out in the DC regime, in which the electrode was vibrating with a frequency of $f_{osc} = 190$ Hz and an amplitude of 100 μm_{pp}. In the DC regime, the SPV signals were excited with the same Xe lamp and a quartz prism monochromator that was also used for the modulated AC regime. The total measurement time of a spectrum in the DC regime was about 30 min. The response time and the measurement resolution of the Kelvin-probe controller were about 0.3 s and 20 μV, respectively, for the given set-up. For comparison, the noise can be significantly below 1 μV for modulated SPV measurements in the fixed capacitor regime.[23] The DC signals were measured with a multimeter (siglent, SDM3065X).

2.4. Combined AC–DC Regime

SPV transients were measured over extremely wide time ranges in the combined AC–DC regime with an oscilloscope for AC in the short time range (ac1 output, Rhode&Schwarz, RTM3004), an oscilloscope for the time range where the AC and DC signals overlap (ac2 and DC outputs, OWON, XDS3302) and a multimeter for the read-out of DC at long times (siglent, SDM3065X). Transients were excited with one single pulse of the Nd:YAG laser described before, i.e., no averaging was carried out. The broadband noise was about 15 mV_{pp} for the combined AC–DC regime due to the vibrating mechanical oscillator.

2.5. Extraction of Transition Energies

It is commonly agreed to extract transition energies as so-called onset-energies from SPV spectra by analyzing changes of the slope.[17] The change of a slope is related to the onset of a new process of photogeneration and charge separation and can be directed toward more positive or negative values of SPV. Here, one has to take care about possible influence of time-dependent relaxation during measurements and about the spectrum of the light source.

2.6. Sample

All measurements were carried out on a β-Ga_2O_3 (001) single crystal doped with Sn and a polished surface (Tamura Corporation, Japan). A preparation of a back contact was not needed, in contrast, for example, to DLTS measurements. Electronic states in the near surface, space charge and bulk regions caused a variability of observable transitions and mechanisms of charge separation and relaxation being an advantage for demonstrating the potential of the nonconventional approach for SPV measurements. All measurements were carried out at room temperature in air.

3. Results and Discussion

3.1. Transient SPV Spectroscopy on β-Ga_2O_3

In **Figure 2**, overview plots of transient SPV spectroscopy are shown. The $K_{ac} \times$ SPV signals ($K_{ac} = 4$) are given in a logarithmic color scale. Transients were measured between 5 ns and 100 ms. In the plots, the onset of the laser pulses was shifted to 20 ns. Incidentally, a negative or a positive sign means that photogenerated electrons (holes) are preferentially separated toward the sample surface (back contact) or toward the back contact (sample surface), respectively.

In the range of photon energies between 0.8 and 1.7 eV (Figure 2a), all signals were within the noise, i.e., no photogeneration followed by charge separation was found. In the range of photon energies between 1.75 and 2.95 eV (Figure 2b), positive SPV signals appeared over the whole spectral range at short times up to several μs (region A), whereas negative signals were present at photon energies above 2.3 eV and at times longer than about 1 μs (region B). In the range of photon energies between 3.1 and 5.8 eV (c), the SPV signals changed the sign depending

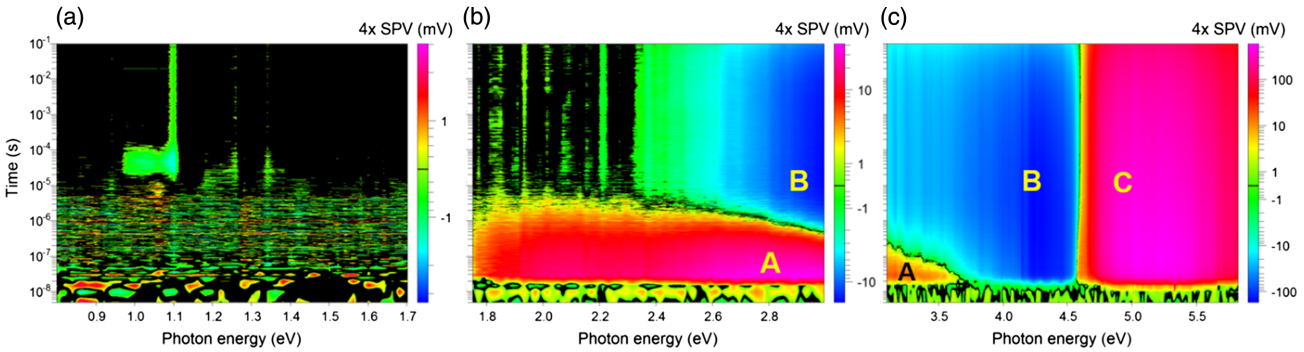

Figure 2. Overview plots of transient SPV spectroscopy in the photon energy–time domain for the ranges of photon energies between a) 0.8 and 1.7 eV, b) 1.75 and 2.95 eV, and c) 3.1 and 5.8 eV. The onset of the laser pulses was shifted to 20 ns. The measurements were carried out up to 100 ms. The SPV signals are given in a logarithmic color scale (blue: negative signals, red: positive signals). The amplification factor was set to 4, i.e., the values of the measured SPV signals have to be divided by 4. A, B, and C denote characteristic regions of A) positive and short, B) negative and long, and C) positive and long SPV signals.

© 2021 The Authors. physica status solidi (a) applications and materials science published by Wiley-VCH GmbH

on photon energy and time. The signals were positive and very small between 3.1 eV ($t \leq 200$ ns) and 3.6 eV ($t \leq 10$ ns, end of region A) and large at photon energies larger than 4.55 eV over the complete time range (region C). The distribution of the negative SPV signals (continuation of region B) continued up to about 4.55 eV over the complete time range excluding the range of times between 200 ns (3.1 eV) and 10 ns (3.6 eV) where the signals were positive. Therefore, three characteristic regions with different dominating charge separation and relaxation processes were distinguished.

SPV transients measured in the AC regime at different excitation wavelengths between 0.8 and 5.8 eV are shown in **Figure 3**. As shown in Figure 2a, no signals were measured for excitation at 0.8 eV. For excitation at 2.27 eV (only region A), the transient could be well fitted with one amplitude (15 mV), one time constant for the increase (7 ns, resolution time of the charge amplifier) and one stretched exponential (time constant τ, stretching parameter β) for the decay ($\tau = 0.7$ µs, $\beta = 0.7$). For excitation at 3.1 eV (superposition of regions A and B), the decay of the transient was given by a superposition of a positive ($\tau = 0.2$ µs, $\beta = 0.4$) and a negative ($\tau = 0.3$ s, $\beta = 0.85$) stretched exponentials whereas the signals at long times were almost limited by the repetition rate of the laser pulses. Therefore, the onset of charge separation resulting in a negative sign of SPV correlated with a decreased value of β corresponding to an increased dispersion of the relaxation of the fast SPV signals with positive sign. For higher photon energies (region C), additional components are required for fits what is out of the scope of the work. One shall also keep in mind that the distributions of positive and negative charge carriers staying separated in space at the moment when the next laser pulse is fired can change for different photon energies (examples for charging at longer times are given in 3.3. and 3.5.) and can therefore change the conditions for charge separation at shorter times.

For explaining the sign of SPV signals and the role of dispersive or trap-limited transport for the relaxation of SPV signals in regions A, B, and C, one shall keep in mind that photogenerated electrons can be separated toward the surface (negative sign) and toward the bulk (positive sign). SPV signals with both signs cannot arise if charge separation takes place only across the surface SCR. Therefore, the schematic band diagram near the surface of β-Ga_2O_3 includes a defective surface region (Δ) and an SCR in the right side of Figure 3. The assumption of a defective surface region with a certain extension is reasonable as the surface of the β-Ga_2O_3 crystal was not intentionally passivated after polishing. Separation and back transport of electrons excited from deep trap states in the bulk into the conduction band (region A) is limited by trapping into unoccupied states near the conduction band edge (E_C, defect states near the band edge are not shown in Figure 3). Back transfer of electrons excited into trap states in the defective surface region and transferred toward the surface (region B) is mainly limited by tunneling between localized states (for example, by Miller–Abrahams tunneling[25]) which can result in long relaxation times already for moderate barrier heights and distances between localized states (see for suitable model considerations also Chapter 4 in the study by Dittrich and Fengler[17]). For strong photogeneration above the bandgap (region C), mobile holes can be separated toward the surface and transferred into localized states in the defective surface region the back transfer from which is limited as well by tunneling between localized states.

The SPV signals obtained at 10 ns, 10 µs, and 10 ms after switching on the laser pulses are shown as spectra in **Figure 4**a. In addition, the intensity spectrum of the laser pulses is given in Figure 4b. Fast positive signals appeared at about 1.7 eV, reached constant values at about 2.1 eV and increased again at photon energies above 2.4 eV until photon energies

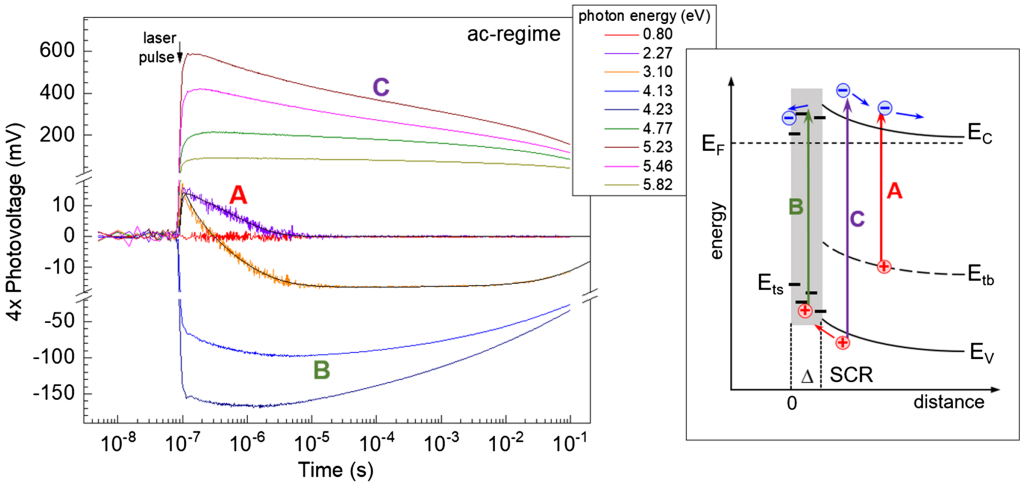

Figure 3. SPV transients measured for excitation at 0.80, 2.27, and 3–10. 4.13, 4.3, 4.77, 5.23, 5.46 and 5.82 eV (red, violet, orange, blue, marine, olive, brown, pink and dark green lines, respectively). The thin black solid lines are fits for excitation at 546 and 400 nm (see also the text). Right side: Schematic band diagram near the surface of β-Ga_2O_3 including charge transfer within a defective surface region (Δ) and charge separation within the space charge region (SCR). SPV transients of regions A, B, and C were limited by transport of electrons in the conduction band (E_C), whereas electrons were excited from deep trap states in the bulk (E_{tb}, positive charge not mobile), by slow back transfer of electrons which were excited into trap states in the defective surface region (E_{ts}) and by slow transfer of photogenerated holes which were transferred from the valence band (E_V) into trap states in the defective surface region, respectively.

© 2021 The Authors. physica status solidi (a) applications and materials science published by Wiley-VCH GmbH

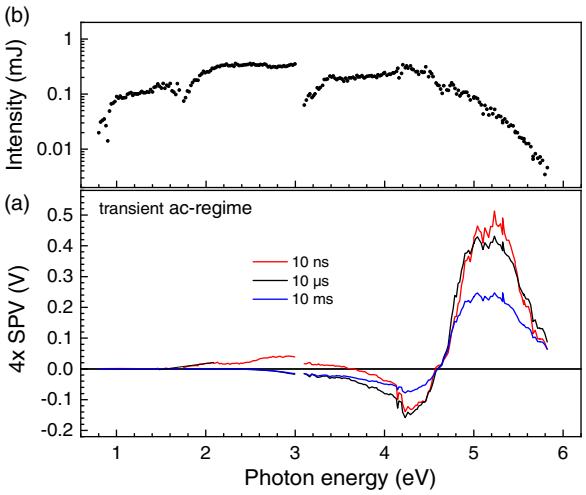

Figure 4. Spectra of the SPV signals deduced at 10 ns, 10 µs, and 10 ms (red, black, and blue lines, respectively) after a) excitation and b) spectrum of the intensity of laser pulses.

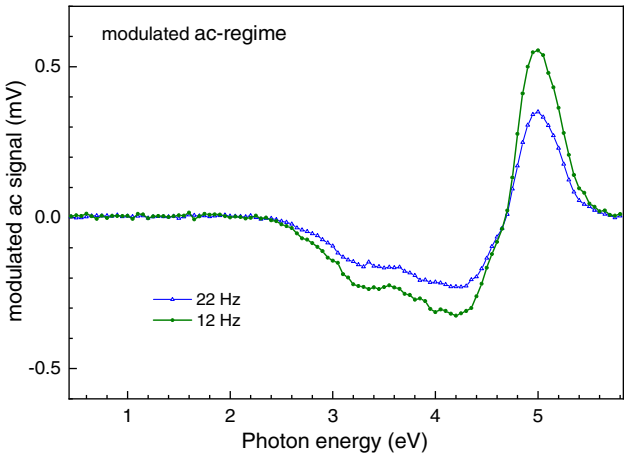

Figure 5. SPV spectra measured in the modulated AC regime at modulation frequencies of 12 and 22 Hz (green line with symbols and blue line with symbols, respectively).

of about 2.7 eV, whereas the laser intensity remained practically constant in the range of the second increase in the fast positive signals.

A decrease of the fast signals toward negative values set on at photon energies of about 3.2 eV and reached a negative maximum at about 4.2 eV. At higher photon energies, the fast signals started to change toward positive sign, whereas the sign changed from negative to positive at about 4.6 eV. The steepest increase in the fast positive signals was observed near the band gap of β-Ga_2O_3. Maximum SPV signals of the order of 120 mV were reached between 5 and 5.3 eV. At higher photon energies, the signals decreased due to the decreasing laser intensity.

The positive signals at about 1.7 and 2.4 eV disappeared in the spectra measured at 10 µs and 10 ms. In contrast, for 10 µs and 10 ms, low negative signals started to appear at photon energies above about 2.5 eV and the negative signals started to increase stronger at photon energies above about 3.4 eV. Incidentally, in this range of increase, the laser intensities changed only little. Above 4.2 eV, the shapes of the spectra were similar for all times of detection. The signals were practically identical for measurements at 10 µs and 10 ms up to about 3.4 eV. For photon energies above 3.4 eV, the signals obtained at 10 ms were about half of the signals measured at 10 µs.

3.2. Modulated SPV Spectroscopy on β-Ga_2O_3

Figure 5 shows SPV spectra of the modulated AC signals for two modulation frequencies. The modulated AC signals were of the order of only hundreds of µV and decreased even further with increasing modulation frequency. This is not surprising with respect to long relaxation times.

The modulated SPV signals started to become negative at a photon energy of about 2.4 eV. At about 3.2 eV, the negative slope became less steep and became again steeper at about 3.55 eV. In the following, the modulated SPV signals changed towards positive at about 4.2 eV, the positive slope increased at about 4.35 eV and increased even more at about 4.6 eV, whereas the maximum slope was reached near 4.75 eV, i.e., close to the bandgap of β-Ga_2O_3.

3.3. DC SPV Spectroscopy on β-Ga_2O_3 in the Kelvin-Probe Mode

SPV spectra were measured in the DC regime in which the electrode was used as a common Kelvin probe. **Figure 6** shows CPD spectra for the virgin, second, and third sweeps, whereas the illumination was off for about 3 min during the time between finishing a spectrum and starting a new one. Incidentally, the given controller was designed in a way that a positive change of the CPD corresponded to a positive SPV signal.

The virgin, i.e., first, spectrum started after relaxation of the CPD to a stable value in the dark (CPD = 0.497 V). A first small change (SPV about 10 mV) toward more positive signals started almost at a photon energy of about 0.8 eV. At higher photon

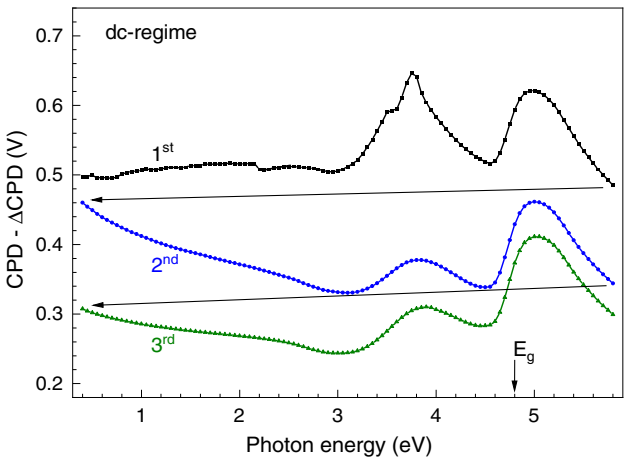

Figure 6. Spectra of the contact potential differences for the first, second, and third sweeps (black, blue, and olive symbols, respectively).

© 2021 The Authors. physica status solidi (a) applications and materials science published by Wiley-VCH GmbH

energies, the CPD continued to increase up to CPD = 0.516 V at photon energy of about 2.15 eV. At 2.2 eV, the CPD decreased by about 8 mV, i.e., the CPD changed toward a negative SPV. Between about 2.5 and 3.0 eV, the signals changed to more negative values (CPD about 0.505 at 3 eV) and increased strongly (SPV about 140 mV) between 2.5 and 3.8 eV (CPD about 0.646 V at 3.8 eV), whereas a pronounced shoulder appeared between 3.5 and 3.6 eV. In the following, the CPD decreased up to 0.517 V at 4.55 eV and increased to 0.622 V at 5.0 eV.

The CPD did not return to the initial value before starting the second and third spectra. Interestingly, instead of relaxing to the initial value before starting the virgin spectrum, the CPD continued strongly to decrease in the spectral range where practically no photosensitivity was observed. Therefore, photogenerated electrons continued to accumulate at the sample surface over a long time. The increase in negative charge at the surface gives evidence that 1) there is a transfer of a fraction of photogenerated electrons from the conduction band into localized states in the defective surface region also for excitation at photon energies above the bandgap, 2) the transfer of electrons toward the surface also continued after switching off the light, i.e., the traps closest to the surface are also the deepest, and 3) the back transfer of electrons from localized states from the defective surface region is the slowest of all relaxation processes (corresponds to region B in Figure 2).

For the second and third spectra, there was no evidence for changes near 0.8 and 2.2 eV and in the region between 3.5 and 3.6 eV. The behavior of the changes near 2.4–2.5 eV (negative change), 3.1–3.2 eV (positive change), around 3.8 eV (negative change) and 4.5–4.6 eV (positive change) was similar for all three spectra. Therefore, these changes can be measured in the DC regime independent of the history of the sample and are therefore characteristic for the given β-Ga_2O_3 crystal with a defective surface region. In contrast, the changes at 0.8, 2.15 and around 3.5–3.6 eV could be detected only for the crystal after prolonged storage in the dark and the occupation state of related defects did not recover within several minutes.

The total change in the CPD was about 200 mV for the starting points of the first and third spectra. A maximum DC SPV can be defined as the difference between CPD at 5.0 and 4.5 eV. The maximum DC SPV increased from 107 mV for the first spectrum to 122 and 128 mV for the second and third spectra, respectively. This increase agrees with ongoing accumulation of negative charge at the surface which causes an increase in surface band bending and is of the same order as for maximum signals in SPV transients.

3.4. SPV Transients on β-Ga_2O_3 over Extremely Wide Time Ranges

Figure 7 shows SPV transients which were measured in the combined AC–DC regime over a very wide time domain for single pulse excitation at 4.43 (Figure 7a) and 5.0 (Figure 7b) eV. The value of K_{ac} was set to 3. At short times, the SPV signals increased to about 25 and 147 mV for 4.43 and 5.0 eV, respectively. At intermediate times, the DC signals increased and the AC signals decayed and oscillated between about 1 and 100 ms due to the vibration of the electrode with $f_{osc} = 190$ Hz and the nulling procedure of the Kelvin-probe controller. At very long times, the DC signals continued to decrease (5.0 eV) and

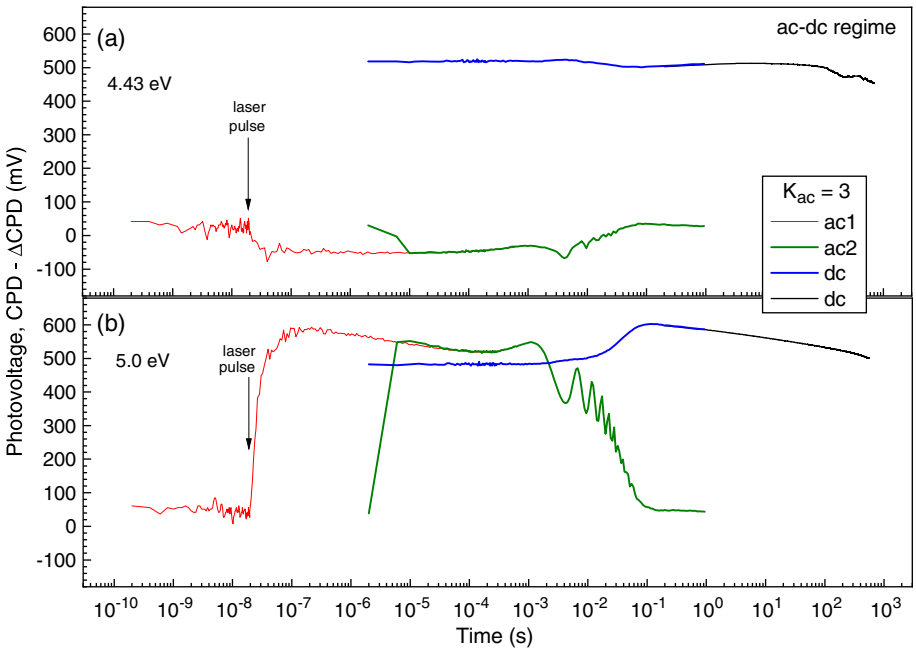

Figure 7. SPV transients measured in the combined AC–DC regime over a very wide time domain for single pulse excitation at 4.43 (Figure 7a) and 5.0 eV (Figure 7b). The logarithmic read-outs were synchronized for two oscilloscopes (ac1 at short times: red lines, ac2 and DC at times where AC and DC signals overlap; green and blue lines, respectively) and a digital multimeter (DC at long times: black lines). The oscillations in the intermediate time range are caused by the variation of the amplification factor due to the periodic change of the distance between the vibrating electrode and the sample surface. The amplification factor was set to 3.

© 2021 The Authors. physica status solidi (a) applications and materials science published by Wiley-VCH GmbH

tended to fluctuate due to ongoing redistribution of photogenerated charge carriers (4.43 eV).

The ac signals depend on the amplification factor. In the combined AC–DC regime, the distance between the surface of the sample and the electrode changes periodically due to the oscillation period of the electrode (f_{osc}). The signal measured by the charge amplifier is proportional to the capacitance between the sample surface and the electrode and therefore to their reciprocal distance. Assuming an ideal sinus modulation of the distance, the AC transient (ac(t)) can be calculated from the measured AC transient ($ac_m(t)$) using the following equation

$$\mathrm{ac}(t) = \frac{(\mathrm{ac_m}(t) - \mathrm{ac_{offset}})}{K_{ac}} \cdot \left(2 - \frac{1}{1 + C_1 \cdot \sin(2\pi \cdot (t - \delta t) \cdot f_{osc})}\right) \tag{1}$$

where C_1 is a factor depending on K_{ac} and δt and ac_{offset} are the phase shift and offset, respectively. The parameters C_1 and δt can be obtained by fitting the AC transients measured in the time domain where the AC and DC signals are overlapping. After that, Equation (1) shall also be applied for the calculation of the SPV signals at the short times.

The complete SPV transient can be reconstructed for the whole very wide time range by applying Equation (1) for ac1 and ac2 and the following equation

$$\mathrm{SPV}(t) = [\mathrm{ac_1}(t)]_{\mathrm{scope1}} + [\mathrm{ac_2}(t) + \mathrm{dc}(t) - \mathrm{dc}(t_0)]_{\mathrm{scope2}} + [\mathrm{dc}(t) - \mathrm{dc}(t_0)]_{\mathrm{mm}} \tag{2}$$

where scope1, scope2, and mm denote the measurement with the first (short times) and second (time range with overlapping AC and DC signals) oscilloscopes and with the multimeter, respectively.

SPV transients reconstructed following Equation (1) and (2) are shown in **Figure 8** for the transients shown in Figure 7. The transients were excited at photon energies above (5.0 eV) and below (4.43 eV) the bandgap of β-Ga_2O_3. For the reconstruction, values of C_1, f_{osc}, and δt of 0.15, 190 Hz, and 2.65 (for 5.0 eV) and 2.6 ms (for 4.43 eV), respectively, were obtained.

For the SPV transient excited at 5.0 eV, the increasing signals at short times are a superposition of two exponentials.

$$\mathrm{SPV}_i(t) = \left[A_1 \cdot \left(1 - \exp\left(-\frac{t - t_0}{\tau_1}\right)\right) + A_2 \cdot \left(1 - \exp\left(-\frac{t - t_0}{\tau_2}\right)\right)\right] \tag{3}$$

A_1, A_2, τ_1, and τ_2 denote the corresponding amplitudes and time constants. The values of τ_1 and τ_2 are 8 and 50 ns, respectively, whereas 8 ns is the resolution time of the ac1 signals in the combined AC–DC regime. The time constant τ_2 describes ongoing charge separation at shorter times caused probably by some retarded charge transfer at/near the interface between Δ and SCR. The same values of τ_1 and τ_2 were used for describing the increasing negative signals of the SPV transient excited at 4.43 eV.

The behavior of the SPV transients at intermediate times can be described, at first glance, by stretched exponentials.

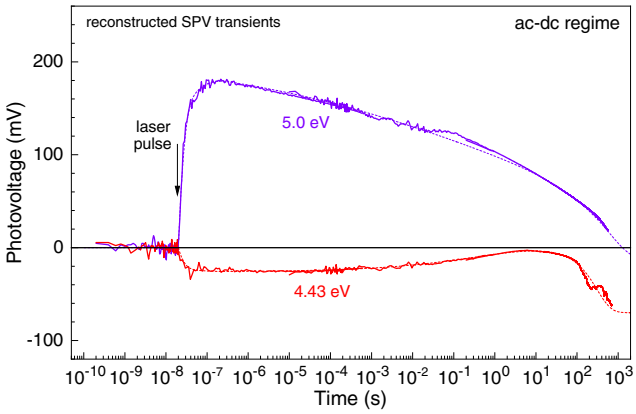

Figure 8. Reconstructed SPV transients for transients shown in Figure 5 (excitation at 4.43 and 5.0 eV: red and violet solid lines, respectively) following the procedure given by Equation (1) and (2), whereas the values of C_1, f_{osc}, and δt were set to 0.15, 190 Hz, and 2.65 (5.0 eV) and 2.6 (4.43 eV) ms, respectively. The violet and red dashed lines give formal fits for the reconstructed transient excited at 5.0 and 4.43 eV, respectively (fit functions were described by an increase at short times, a decay by stretched exponentials at intermediate times and a logistic growth function at long times).

The corresponding time constants and stretching parameters are 0.1 s and 0.12 and 400 s and 0.5 for excitation at 5.0 eV (2 stretched exponentials) and 0.4 s and 0.3 for excitation at 4.43 eV (one stretched exponential). The two relaxation processes found for excitation at 5.0 eV (region C) can be assigned to a back transfer of electrons toward the surface and of holes from the defective surface region into the bulk. The relaxation process found for excitation at 4.43 eV (region B) can be assigned to back transfer of electrons from the defective surface region into the bulk.

At long times, at first glance, a logistic growth function with negative sign and time constants of about 500 s for excitation at 5.0 eV and 200 s for excitation at 4.43 eV had to be considered. Incidentally, the presence of a logistic growth function at long times gives evidence for very slow charge separation processes, probably due to very slow relaxation of charge trapped at surface states. Regarding to the negative sign of this process, the relaxation of trapped holes is faster so that negatively charged surface defects stay what has been observed for β-Ga_2O_3 by X-ray photoemission spectroscopy.[26] This is also in agreement with the negative net charging in the experiments in the dc-regime (Figure 6).

3.5. Analysis of Transition Energies and Franck–Condon Shifts

The strongest change and the highest positive SPV signals appeared in the region near the bandgap of β-Ga_2O_3 for the measurements in the transient and modulated AC regimes and in the DC regime (the β-Ga_2O_3 crystal behaves as a n-type semiconductor with a depletion layer). A variability of transitions which could be distinguished in the different measurement regimes is shown in **Figure 9** comparing SPV spectra measured in the transient and modulated AC regimes with detection time of 10 ns and

© 2021 The Authors. physica status solidi (a) applications and materials science published by Wiley-VCH GmbH

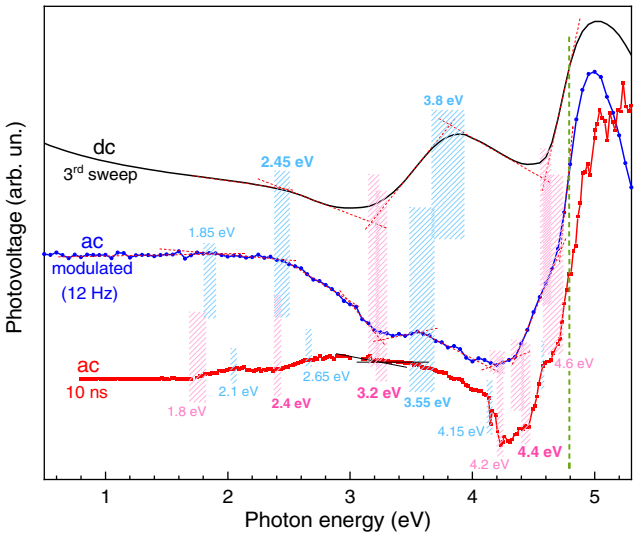

Figure 9. Variability of transition energies in the β-Ga_2O_3 crystal obtained by measurements in the transient AC regime (red line with symbols), in the modulated AC regime (purple line with symbols) and in the DC regime (black line). The values given in blue and pink colors are assigned to transitions resulting in changes toward more negative or positive SPV signals. The spectra were scaled differently to compare the shapes directly.

modulation frequency of 12 Hz, respectively, and in the DC regime (third spectrum). As already mentioned, the shapes of the spectra could be rather different depending on the measurement regime.

The onset energy of 3.2 eV of the change of the SPV signals toward a more positive direction was similar for all regimes. This transition has not been described by DLTS measurements.[12,13] Furthermore, this transition is close to the predicted energy of 3.31 eV for the oxygen vacancy in the O(I) position β-Ga_2O_3.[5,27]

Positive (transient AC regime) or negative (modulated AC regime and DC regime) changes of the signals at 2.4–2.45 eV give evidence that photogeneration from similar electronic states near the midgap of β-Ga_2O_3 can result in opposite directions of charge separation. Such a difference is caused by the variation of the quasistatic distribution of charge across the interface between the Δ and SCR under different illumination conditions leading to preferential separation of photogenerated electrons toward the bulk or toward the surface, respectively.

An important question is how transitions obtained in the coarse way shown in Figure 9 can be compared with transitions obtained by other techniques. The determination of precise transition energies from SPV spectra can be challenging as, aside photogeneration and recombination, numerous processes with different directions of charge separation and with very different time scales can be involved in the formation and relaxation of SPV signals. This is in contrast to absorption spectroscopy and DLTS for which transition energies are well defined by optical or thermal excitation, respectively. Furthermore, also deep-level optical spectroscopy (DLOS) can provide well defined transition energies if considering the redistribution of photogenerated charge across an SCR.

In the ideal case, an SPV spectrum is dominated by one generation spectrum in the spectral range of the corresponding transition. However, as shown in Figure 8, charging processes can overlay over time scales which can be even longer than the measurement time of a spectrum. This needs sophisticated simulation and fitting procedures especially for SPV spectra measured in the DC regime. The direct influence of slow charge transfer processes is eliminated in the transient and modulated AC regimes. This means that the spectral range around one transition energy is dominated by only one generation spectrum at first glance. In such a case, a minimum number of transitions can be defined and analyzed. **Figure 10** shows SPV spectra of β-Ga_2O_3 measured in transient and modulated AC regimes. Four transitions resulting in positive SPV signals (P1–P4) and three transitions resulting in negative SPV signals (N1–N3) have been distinguished, whereas P1 and P2 were observed only after very short relaxation times; P3, P4, N1, and N3 were observed in all SPV spectra and a clear signature for N2 was not found in the SPV spectrum measured in the modulated AC regime.

The shape of a range of one transition in a SPV spectrum can be fitted by the shape of one absorption cross section if assuming that there is no other transition involved and that the SPV signal is proportional to absorption. The dependence of an absorption cross section (σ) on photon energy (E_{ph}) is defined by an integral over energy (E), a broadening parameter (Γ), absorption energy (E_{abs})[28]

$$\sigma(E_{ph}) \sim \int_0^{\infty} \frac{\exp(-[E + E_{abs} - E_{ph}]^2/\Gamma^2) \cdot \sqrt{E} \cdot dE}{E_{ph} \cdot (E + E_{abs})^2} \tag{4}$$

The transitions in the spectra shown in Figure 10 were fitted using Equation (4). The values of E_{abs} and Γ are shown in **Table 1** for the corresponding transitions P1–P4 and N1–N3. As remark, one shall keep in mind, that those values can also be understood as rough estimates due to the complexity of the formation of SPV signals.

The transition at 4.42–4.47 eV can be related to the transition $E_C - 4.4$ eV, which was found in all β-Ga_2O_3 crystals investigated by DLOS.[29] In the following, the Franck–Condon shift (d_{FC}) will be obtained for this defect from Γ (0.1 eV). Following Alkauskas et al.,[28] Γ depends on the phonon energies in the ground and excited states (assumption: $E_{ph,g} = E_{ph,e} = E_{ph,0}$), d_{FC} and temperature (T) as

$$\Gamma = \sqrt{2 \cdot d_{FC} \cdot E_{ph,0}} \cdot \sqrt{\coth(E_{ph,0}/k_B T)} \tag{5}$$

where k_B denotes the Boltzmann constant.

Figure 11a shows the dependence of Γ on E_{ph} for different values of d_{FC}. Vice versa, a Franck–Condon shift can be obtained if Γ and the phonon energy are known. A typical Raman spectrum for a β-Ga_2O_3 crystal is shown in Figure 11b. The phonon energies of this spectrum were used to calculate d_{FC} for $\Gamma = 0.1$ eV (shown also in Figure 11b).

Ghadi et al. found that the Franck–Condon shift of this defect transition is 0.06 eV.[29] This value is reached around the phonon modes $A_g^{(8)}$ and $B_g^{(5)}$ that occur at wavenumbers of 631 and 652 cm^{-1}. This strongly suggests that the phonon modes $A_g^{(8)}$ and $B_g^{(5)}$ are mainly involved in the absorption cross section of the defect at E_C – (4.4 … 4.47) eV.

© 2021 The Authors. physica status solidi (a) applications and materials science published by Wiley-VCH GmbH

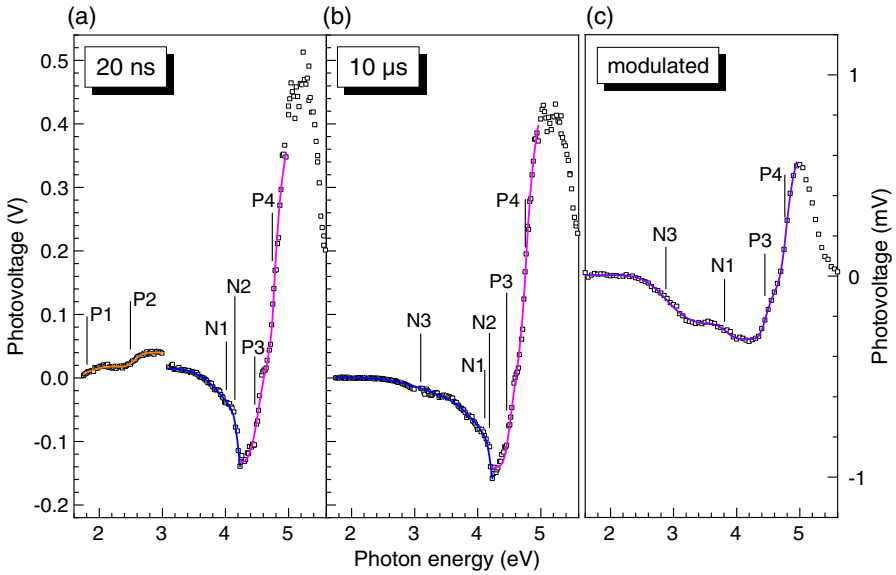

Figure 10. SPV spectra of β-Ga_2O_3 measured in transient (measured at a) 20 ns and b) 10 µs after excitation) and c) modulated AC regimes. P1–P4 and N1–N3 denote transitions which cause positive or negative SPV signals, respectively. Positive or negative SPV signals can be assigned to processes dominated by charge separation across the surface SCR or by electron transfer toward the surface through the defective surface region, respectively (see also Figure 3). The solid lines are fits in which only proportionalities to absorption cross sections have been considered.

Table 1. Transition energies and broadening parameters obtained by fitting the SPV spectra shown in Figure 10 with shapes of absorption cross sections.

Transition	Transient AC regime		Modulated AC regime	
	E_{abs} [eV]	Γ [eV]	E_{abs} [eV]	Γ [eV]
P1	1.76	0.29	–	–
P2	2.48	0.1	–	–
P3	4.47	0.11	4.42	0.095
P4	4.74	0.07	4.74	0.08
N1	4.05	0.5	–	–
N2	4.18	0.06	3.76	0.15
N3	3.09	0.62	2.84	0.4

4. Conclusions

SPV spectra were measured by a nonconventional approach on the ultrawide bandgap semiconductor β-Ga_2O_3 with the same gold mesh electrode over a very wide range of photon energies and over wide time domains in the transient AC (10 ns to 1 s, transient SPV spectroscopy), modulated AC (modulated SPV spectroscopy with low noise), and DC (above 1 s, SPV spectroscopy in the mode of a Kelvin probe) regimes. Furthermore, for excitation at different photon energies, the measurement and reconstruction of SPV transients, which were excited with one single pulse, over a very wide time range (10 ns to 1000 s and longer) was demonstrated for the combined AC–DC regime.

The nonconventional approach is based on the highly sensitive measurement of charge appearing on the measurement

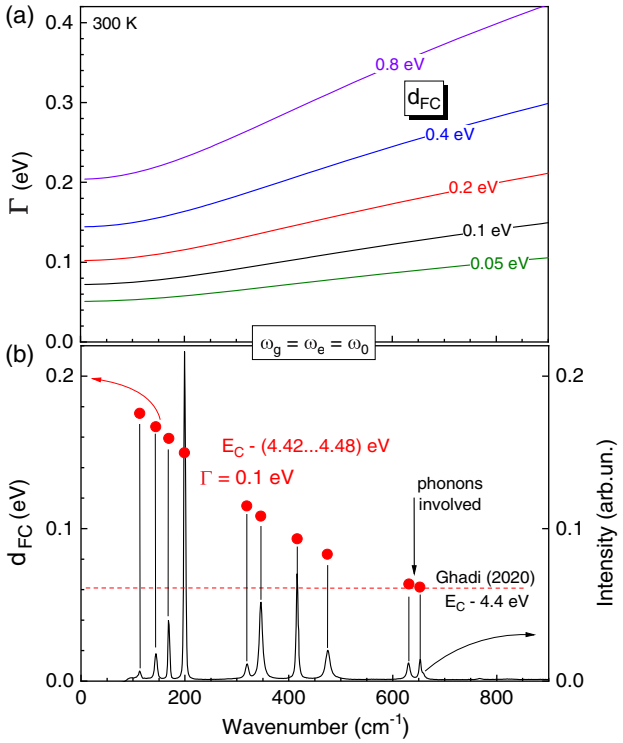

Figure 11. a) Dependence of the broadening parameter (Γ) on the wavenumber (*a*) for different values of the Franck–Condon shift following Equation (4) and typical Raman spectrum of a β-Ga_2O_3 crystal and values of the Franck–Condon shifts (d_{FC}) for the corresponding phonon energies for b) Γ = 0.1 eV. The dashed line gives the value of d_{FC} obtained by Ghadi et al.[29]

© 2021 The Authors. physica status solidi (a) applications and materials science published by Wiley-VCH GmbH

capacitor during the evolution of SPV signals. SPV measurements in the combined AC–DC regime are not possible using conventional SPV measurement principles with capacitive outcoupling of SPV signals and a Kelvin-probe. However, due to a lower measurement capacitance, it seems unrealistic to reach with the nonconventional approach noise levels as low as for SPV measurements with capacitive outcoupling. Therefore, the traditional fixed capacitor with a buffer will remain important especially for separate and relatively fast modulated SPV measurements on common photoactive materials, such as TiO_2, $BiVO_4$, or Cu_2O. Furthermore, in comparison with SPV measurements with a fixed capacitor in ultrahigh vacuum,[30] treated surfaces are not in mechanical contact with an insulator for the nonconventional approach what is a big advantage for its future application in ultrahigh vacuum.

Several electronic transitions were distinguished for β-Ga_2O_3 which depended also on the measurement conditions. As remark, the detailed analysis of related SPV spectra is challenging since different regions in the sample may contribute differently to the SPV signals in the different measurement regimes due to different charging, charge transport, and distributions of electronic states in the sample. An accumulation of negative charge at the surface was observed at long times independent whether the SPV signals were positive or negative before. The situation will be even more complex for the engineering of electronic transitions and bandgaps by alloying Ga_2O_3, for example with aluminum,[31] iron,[32] or titanium.[33] But nevertheless, related samples can be studied by the nonconventional approach of SPV measurements proposed in this work. For example, several transition energies and broadening parameters have been obtained or estimated for β-Ga_2O_3 by fitting positive and negative slopes of transient and modulated SPV spectra in the AC regime.

Finally, the nonconventional approach of measuring SPV signals over wide ranges in photon energy and time opens new opportunities for investigating electronic properties in semiconductors with ultrawide bandgaps and any other photoactive material. Furthermore, this approach can also be applied for excitation with electrical current pulses, i.e., also phenomena related to potential changes in charge storage materials can be studied.

Acknowledgements

S.F. is grateful to the AiF Project GmbH (KK5123601DF0) for financial support. The authors are grateful to Dr. M. Franke for the development of the analog electronics of the set-up and for discussions about measurement principles and to C. Olesch for developing a software for synchronized transient measurements with several devices. Furthermore, the authors are grateful to the reviewers for inspiring questions.

Open access funding enabled and organized by Projekt DEAL.

Conflict of Interest

The authors declare no conflict of interest.

Data Availability Statement

The data that support the findings of this study are available from the corresponding author upon reasonable request.

Keywords

gallium oxide, surface photovoltage spectroscopy, very wide bandgaps, wide time domains

Received: March 30, 2021
Revised: June 1, 2021
Published online: July 31, 2021

[1] J. Y. Tsao, S. Chowdhury, M. A. Hollis, D. Jena, N. M. Johnson, K. A. Jones, R. J. Kaplar, S. Rajan, C. G. Van de Walle, E. Bellotti, C. L. Chua, R. Collazo, M. E. Coltrin, J. A. Cooper, K. R. Evans, S. Graham, T. A. Grotjohn, E. R. Heller, M. Higashiwaki, M. S. Islam, P. W. Juodwlkis, M. A. Khan, A. D. Koehler, J. H. Leach, U. K. Mishra, R. J. Nemanich, R. C. N. Pilawa-Podgurski, J. B. Shealy, Z. Sitar, M. J. Tadjer, et al., *Adv. Electron. Mater.* **2018**, *4*, 1600501.
[2] S. J. Pearton, J. Yang, P. H. Cary IV, F. Ren, J. Kim, M. J. Tadjer, M. A. Mastro, *Appl. Phys. Rev.* **2018**, *5*, 011301.
[3] H. W. Xue, Q. M. He, G. Z. Jian, S. B. Long, T. Pang, M. Liu, *Nanoscale Res. Lett.* **2018**, *13*, 290.
[4] S. Garud, N. Campa, T. G. Allen, R. Kotipalli, D. Flandre, M. Batuk, J. Hadermann, M. Meuris, J. Poortmans, A. Smets, B. Vermang, *Phys. Stat. Solidi A* **2018**, *215*, 1700826.
[5] T. G. Allen, M. Ernst, C. Samundsett, A. Cuevas, *IEEE J. Photovolt.* **2015**, *6*, 1586.
[6] D. Chua, S. B. Kim, R. Gordon, *AIP Adv.* **2019**, *9*, 055203.
[7] G. W. Busser, B. Mei, A. Pougin, J. Strunk, R. Gutkowski, W. Schuhmann, M.-G. Willinger, R. Schlögl, M. Muhler, *ChemSusChem* **2014**, *7*, 1030.
[8] X. Wang, Q. Xu, M. Li, S. Shen, X. Wang, Y. Wang, Z. Feng, J. Shi, H. Han, C. Li, *Angew. Chem., Int. Ed.* **2012**, *51*, 13089.
[9] M.-G. Ju, X. Wang, W. Liang, Y. Zhao, C. Li, *J. Mater. Chem. A* **2014**, *2*, 17005.
[10] X. Wang, S. Shen, S. Jin, J. Yang, M. Li, X. Wang, H. Han, C. Li, *Phys. Chem. Chem. Phys.* **2013**, *15*, 19380.
[11] Y. Wang, P. Zhuang, H. You, H. Dong, X. Zhou, *J. Phys. Chem. C* **2019**, *123*, 8990.
[12] K. Irmscher, Z. Galazka, M. Pietsch, R. Uecker, R. Fornari, *J. Appl. Phys.* **2011**, *110*, 063720.
[13] Z. Zhang, E. Farzana, A. R. Arehart, S. A. Ringel, *Appl. Phys. Lett.* **2016**, *108*, 052105.
[14] A. T. Neal, S. Mou, S. Rafique, H. Zhao, E. Ahmadi, J. S. Speck, K. T. Stevens, J. D. Blevins, D. B. Thomson, N. Moser, K. D. Chabak, G. H. Jessen, *Appl. Phys. Lett.* **2018**, *113*, 062101.
[15] H. Gao, S. Muralidharan, N. Pronin, M. R. Karim, S. M. White, T. Asel, G. Foster, S. Krishnamoorthy, S. Rajan, L. R. Cao, M. Higashiwaki, H. von Wenckstern, M. Grundmann, H. Zhao, D. C. Look, L. Brillson, *Appl. Phys. Lett.* **2018**, *112*, 242102.
[16] L. Kronik, Y. Shapira, *Surf. Sci. Rep.* **1999**, *37*, 1.
[17] T. Dittrich, S. Fengler, *Surface Photovoltage Analysis of Photoactive Materials*, World Scientific Publishing Europe Ltd., London, UK **2020**.
[18] S. Fengler, H. Kriegel, M. Schieda, H. Gutzmann, T. Klassen, M. Wollgarten, T. Dittrich, *ACS Appl. Mater. Interfaces* **2020**, *12*, 3140.
[19] A. Song, I. Levine, R. van de Krol, T. Dittrich, S. P. Berglund, *Chem. Soc.* **2020**, *11*, 11195.
[20] I. Levine, I. Gamov, M. Rusu, K. Irmscher, C. Merschjann, E. Richter, M. Weyers, T. Dittrich, *Phys. Rev. B* **2020**, *101*, 245205.
[21] V. Duzhko, V. Y. Timoshenko, F. Koch, T. Dittrich, *Phys. Rev. B* **2001**, *64*, 075204.
[22] T. Dittrich, O. Garcia Vera, S. Fengler, S. Pineda, S. Bönisch, *Rev. Sci. Instrum.* **2019**, *90*, 026102.

© 2021 The Authors. physica status solidi (a) applications and materials science published by Wiley-VCH GmbH

[23] I. Levine, O. Garcia Vera, M. Kulbak, D.-R. Ceratti, C. Rehermann, J. A. Marquez, S. Levcenko, T. Unold, G. Hodes, I. Balberg, D. Cahen, T. Dittrich, *ACS Energy Lett.* **2019**, *4*, 1150.
[24] T. Dittrich, M. Franke (Helmholtz-Zentrum Berlin für Materialien und Energie GmbH) DE 10 2019 117989 B3, 2020, WO 2021/000998 A1, **2021**.
[25] A. Miller, E. Abrahams, *Phys. Rev.* **1960**, *120*, 745.
[26] T. C. Lovejoy, R. Chen, X. Zheng, E. G. Villora, K. Shimamura, H. Yoshikawa, Y. Yamashita, S. Ueda, K. Kobayashi, S. T. Dunham, F. S. Ohuchi, M. A. Olmstead, *Appl. Phys. Lett.* **2012**, *100*, 181602.
[27] J. B. Varley, J. R. Weber, A. Janotti, C. G. Van de Walle, *Appl. Phys. Lett.* **2010**, *97*, 142106.
[28] A. Alkauskas, M. D. McCluskey, C. G. Van de Walle, *J. Appl. Phys.* **2016**, *119*, 181101.
[29] H. Ghadi, J. F. McGlone, C. M. Jackson, E. Farzana, Z. Feng, A. F. M. Anhar Uddin Bhuiyan, H. Zhao, A. R. Arehart, S. A. Ringel, *APL Mater.* **2020**, *8*, 021111.
[30] V. Parvan, A. Mizrak, I. Majumdar, B. Ümsür, W. Calvet, D. Greiner, C. A. Kaufmann, T. Dittrich, E. Avancini, I. Lauermann, *Appl. Surf. Sci.* **2018**, *444*, 436.
[31] T. Minami, Y. Nishi, T. Miyata, *Appl. Phys. Express* **2015**, *8*, 022301.
[32] A. Barthel, J. Roberts, M. Napari, M. Frentrup, T. Huq, A. Kovacs, R. Oliver, P. Chalker, T. Sajavaara, F. Massabuau, *Micromachines* **2020**, *11*, 1128.
[33] B. Mallesham, S. Roy, S. Bose, A. N. Nair, S. Sreenivasan, V. Shuttanandan, C. V. Ramana, *ACS Omega* **2020**, *5*, 104.

© 2021 The Authors. physica status solidi (a) applications and materials science published by Wiley-VCH GmbH